Temperature Dependence of the Half-Integer Magnetic Flux Quantum

J. R. Kirtley,[1*] C. C. Tsuei,[1] K. A. Moler[2]

The temperature dependence of the half-integer magnetic flux quantum effect in thin-film tricrystal samples of the high-critical-temperature cuprate superconductor $YBa_2Cu_3O_{7-\delta}$ was measured and found to persist from a temperature of 0.5 kelvin through a critical temperature of about 90 kelvin, with no change in total flux. This result implies that *d*-wave symmetry pairing predominates in this cuprate, with a small component of time-reversal symmetry breaking, if any, over the entire temperature range.

An important development in the understanding of the superconducting state in high-critical-temperature cuprate superconductors has been the demonstration that the Cooper pairing in several of the hole-doped cuprates has predominately *d*-wave symmetry (*1*). However, although this pairing symmetry implies that the pairing interaction has certain characteristics (*2*), it does not specifically identify the mechanism responsible for high-temperature superconductivity. It is unclear whether *d*-wave symmetry predominates in all of the cuprate superconductors, whether there is a dependence of the symmetry on doping, or whether there is a temperature dependence of the pairing symmetry; the extent of a possible *s*-wave component is also uncertain. There is reason to think that the electron-doped cuprate $Nd_{1.85}Ce_{0.15}CuO_{4-y}$ may have *s* symmetry (*3*), and there have been reports of a change in symmetry in $Bi_2Sr_2CaCu_2O_{8+\delta}$ as a function of temperature (*4*) and doping (*5*). It has been suggested that, in the cuprates, there may be a nearly balanced competition between *s*- and *d*-wave pairing, in which either may predominate, depending on the details of the band structure (*6*).

The question of the temperature dependence of the order-parameter symmetry is important for several reasons. First, any deviation from predominately *d*-wave pairing as a function of temperature would be an important clue to the pairing mechanism in high-temperature superconductors. In particular, such an observation would be evidence against a spin-mediated pairing mechanism (*7, 8*). Second, although it appears unlikely that there is substantial time-reversal symmetry breaking (*9*) in the pairing in the bulk of the cuprate superconductors (*10–12*), it has been proposed that such symmetry breaking can occur at twin and grain boundaries (*13, 14*) or at the interface between $YBa_2Cu_3O_{7-\delta}$ (YBCO) and a conventional superconductor (Pb) (*15*). The time-reversal symmetry breaking component could introduce a temperature dependence to the pairing symmetry: There have been reports of a temperature-dependent time-reversal symmetry breaking component to the pairing in YBCO near the critical temperature T_c (*16*) and a report of a phase transition in $Bi_2Sr_2CaCu_2O_8$ at low temperatures, which may indicate a second component to the order parameter (*17*). It is therefore important to conclusively determine whether time-reversal symmetry breaking occurs at any temperature in the cuprate superconductors.

However, it is difficult to probe the temperature dependence of the pairing symmetry in unconventional superconductors, as all the techniques used so far become obscured by thermal excitations at higher temperatures. Although phase-sensitive tests that depend on Josephson pair tunneling (*10, 11, 18–21*) are in principle immune to thermal broadening, in practice most of these tests also fail at higher temperatures because they involve tunneling into low-T_c superconductors.

To the best of our knowledge, only experiments that involve grain-boundary Josephson junctions in the cuprates (*20, 21*), in which the entire structure is made of high-critical-temperature superconductors, can be used to determine pairing symmetry at all temperatures through T_c. However, even this class of experiments presents difficulties. The best way to make a symmetry test with these samples is to magnetically image the half-flux quantum effect (*20*). The most sensitive detectors for such imaging are low-T_c superconducting quantum interference devices (SQUIDs), which fail to operate above ~9 K. We have avoided the problem of the low critical temperature of our SQUID sensors by building a microscope in which the sample is heated while the SQUID is kept cold (*22*). This allows us to warm the sample to temperatures as high as 150 K while the SQUID continues to operate (*23*).

The tricrystal experimental geometry we used has been described previously (*20, 24*). A 300-nm-thick film of YBCO was grown epitaxially on a tricrystal substrate of $SrTiO_3$. The crystalline orientations of the tricrystal were chosen (Fig. 1A) to form an energetically frustrated state at the tricrystal point for a superconductor with $d_{x^2-y^2}$ pairing symmetry. The frustration is relaxed by the spontaneous generation of a magnetic vortex at the tricrystal point with total flux $hc/4e$ (where h is Planck's constant, c is the speed of light, and e is the charge on the electron), which is half that of a conventional superconducting vortex. The presence of this half-vortex is perhaps the most conclusive evidence to date for predominately *d*-wave superconductivity in the cuprate superconductors.

Scanning SQUID microscope images from our tricrystal samples were taken above 4.2 K with a relatively large pickup loop (17.8 μm on a side) (Fig. 1B) to minimize the effects of errors in the positioning of the sensor. The data below 4 K were taken with a 7.5-μm square loop with He_3 as the cryogen. The images (Fig. 1C) were taken with the sample in nominal zero field, as confirmed by the absence of bulk Abrikosov vortices in the vicinity of the tricrystal point

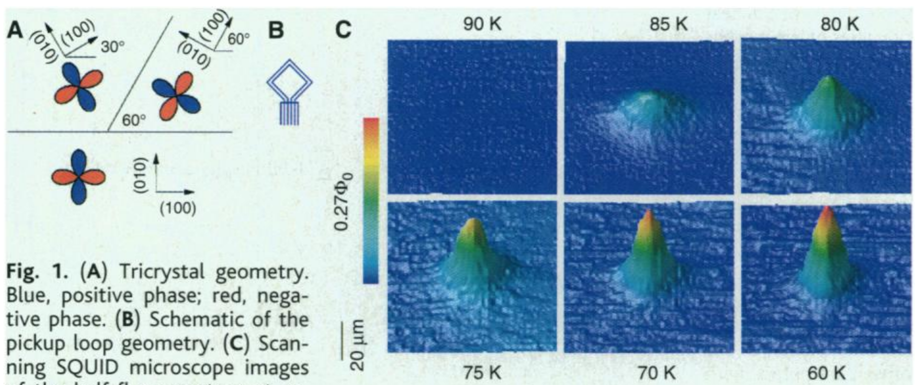

Fig. 1. (**A**) Tricrystal geometry. Blue, positive phase; red, negative phase. (**B**) Schematic of the pickup loop geometry. (**C**) Scanning SQUID microscope images of the half-flux quantum at selected temperatures.

[1]IBM T. J. Watson Research Center, Post Office Box 218, Yorktown Heights, NY 10598, USA. [2]Department of Applied Physics, Stanford University, Stanford, CA 94305, USA.

*To whom correspondence should be addressed. E-mail: kirtley@us.ibm.com

after cooldown. Magnetic flux is spontaneously generated at the tricrystal point as the sample is cooled through T_c. Close to T_c, the vortex is broad, with a reduced peak intensity because the magnetic flux penetrates along the sample grain boundaries. As the temperature is reduced, the vortex image becomes sharper.

Although the SQUID signal directly above an Abrikosov vortex that is trapped away from the tricrystal point is twice as large as that above the half-vortex flux quantum at low temperatures (Fig. 2A), closer examination shows that the temperature dependences are different near T_c. Nevertheless, spontaneous magnetization at the tricrystal point persists at all temperatures from 0.5 K through T_c, implying that the frustration built into the superconductor at the tricrystal point exists at all temperatures, which in turn suggests that *d*-wave pairing predominates at all temperatures. Furthermore, there were occasional random changes observed in the sign of the vortex when measurements were made close to T_c, presumably due to interactions with the SQUID during scanning. The absolute magnitude of the SQUID signal was unchanged by these sign changes, indicating that a component of time-reversal symmetry breaking, if present, was small.

We think that the difference between the temperature dependences of the SQUID peak signal for the two types of vortices resulted from the different temperature dependences of the London penetration depth, which controls the peak field strength of the Abrikosov vortex, and the Josephson penetration depth, which controls the peak field of the half-vortex. However, a temperature-dependent imaginary component to the order parameter could also change the peak field above the half-vortex. Distinguishing between these two effects requires detailed modeling.

We modeled the grain boundaries making up the tricrystal point as wedges of superconductors centered about the tricrystal meeting line $x = 0$, $y = 0$, z. The magnetic fields for a Josephson vortex at the tricrystal line are given by (*24*)

$$B_z(r_i, r_\perp) = \frac{2\Phi_0 a_i}{\pi\lambda_{ab}\lambda_{Ji}} \frac{e^{-r_i/\lambda_{Ji}}}{1 + a_i^2 e^{-2r_i/\lambda_{Ji}}} e^{-r_\perp/\lambda_{ab}} \qquad (1)$$

where λ_{ab} is the in-plane London penetration depth, λ_{Ji} is the Josephson penetration depth of the *i*th grain boundary, $\Phi_0 = hc/2e$ is the superconducting flux quantum, r_i is the distance along the *i*th grain boundary, $r_\perp$ is the distance perpendicular to the grain boundary, and a_i is a normalization constant such that $a_i/[\lambda_{Ji}(1 + a_i^2)]$ is the same for all three grain boundaries; the total flux at the tricrystal point is $\Phi = \Sigma_i(\Phi_0/2\pi)4\ \tan^{-1}(a_i)$. Once the fields at the surface of the grain boundary are calculated, the fields at height z above the surface are determined (for fields derived from a two-dimensional current distribution) by

$$b_z(k_x, k_y, z) = \exp(-\sqrt{k_x^2 + k_y^2}\,z)\, b_z(k_x, k_y, 0) \qquad (2)$$

where b_z is the two-dimensional Fourier transform of the field $B_z(\vec{r})$ and k_x and k_y are the wave vectors in the x and y directions, respectively (*25*). This treatment neglects the effects of overlapping of fields from different grain boundaries close to the tricrystal point and does not take into account modifications to the fields due to the finite thickness of the cuprate films. The fields at a height z above the sample are integrated over the known pickup loop geometry to obtain the SQUID flux as a function of scanning position.

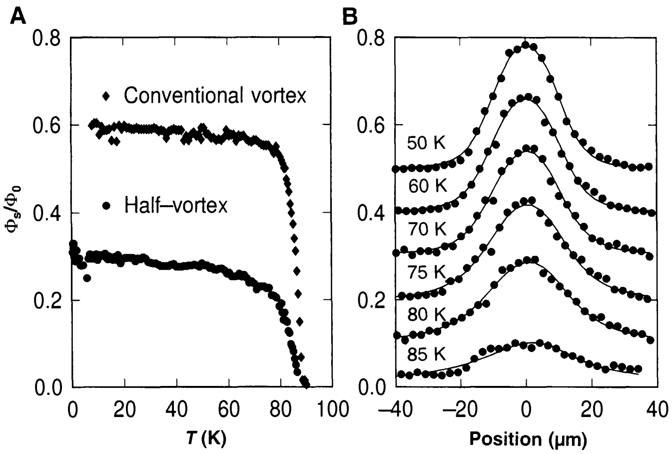

Fig. 2. (**A**) Comparison of the temperature dependence of the flux through the SQUID pickup loop Φ_s, with the loop directly above a conventional vortex and the half-vortex. The pickup loops do not capture all of the flux from the vortices, even when directly above their centers, because of their finite spacing from the sample surface. (**B**) The dots are horizontal cross sections through the center of the half-vortex, for a number of temperatures. The lines are fits to the data with the grain-boundary Josephson penetration depth λ_J and total flux Φ as fitting parameters. The best fit values are as follows: $\lambda_J = 3.3\ \mu$m, $\Phi = 0.48\Phi_0$ ($T = 50$ K); $\lambda_J = 4.2\ \mu$m, $\Phi = 0.50\Phi_0$ ($T = 60$ K); $\lambda_J = 5.0\ \mu$m, $\Phi = 0.50\Phi_0$ ($T = 70$ K); $\lambda_J = 7.7\ \mu$m, $\Phi = 0.48\Phi_0$ ($T = 75$ K); $\lambda_J = 9.5\ \mu$m, $\Phi = 0.52\Phi_0$ ($T = 80$ K); and $\lambda_J = 18.3\ \mu$m, $\Phi = 0.65\Phi_0$ ($T = 85$ K).

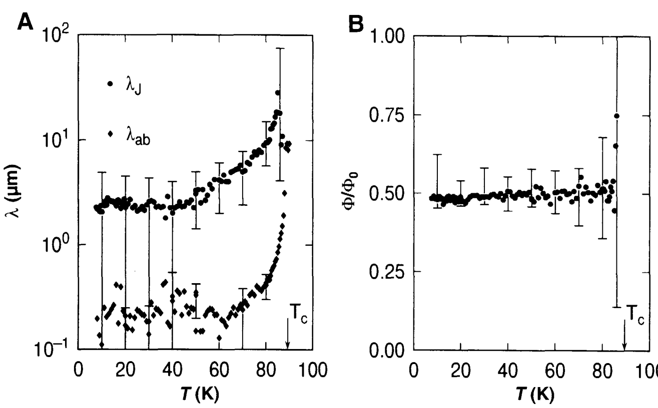

Fig. 3. (**A**) Temperature dependence of the best fit values of the Josephson penetration depth λ_J and London penetration depth λ_{ab}. (**B**) Temperature dependence of our fit values for the total flux Φ spontaneously generated at the tricrystal point. Error bars are assigned by varying the parameter of interest, finding a least squares fit as a function of the other parameters, with a criterion of a doubling of χ^2 between fit and experimental values.

The dots in Fig. 2B show cross sections through the centers of the vortex images of Fig. 1C parallel to the horizontal grain boundary (Fig. 1A), and the lines are fits to these data with the model described above. The height z of the SQUID above the sample surface was chosen by fitting Abrikosov vortex data as described previously (*22*), assuming an average low-temperature London penetration depth of $\lambda_{ab} = 0.15\ \mu$m and a fixed total flux in the vortex of $\Phi_0 = hc/2e$. This gave $z = 4.4\ \mu$m for the 17.8-μm pickup loop data and $z = 1.2\ \mu$m for the 7.5-μm pickup loop data. The full set of temperature-dependent data for the Abrikosov vortices was fit keeping this value of z fixed, with the in-plane penetration depth λ_{ab}, a horizontal peak position, and a flux background as fitting parameters. The best fit values for $\lambda_{ab}(T)$ are plotted in Fig. 3. The half-flux quantum data were fit with z fixed and λ_{ab} determined from fits to Abrikosov vortices, with four fitting parameters: the total flux Φ in the vortex, the Josephson penetration depth λ_J (assumed to be the same for all three grain boundaries), a horizontal peak position, and a flux background. A representative sampling of these fits is shown in Fig. 2B. The fit values for λ_J and Φ are given in Fig. 3.

The persistence of spontaneous magnetization at all temperatures up to T_c in our tricrystal samples implies that d-wave symmetry predominates throughout. Our modeling gives best fit values of $\Phi = \Phi_0/2$ to within $\pm 10\%$ for all temperatures up to $T = 84$ K, ~ 6 K below T_c. Above this temperature, the Josephson penetration depths become very long, producing uncertainties in the fit parameters that diverge closer to T_c. To within the uncertainties assigned by our statistical analysis (as indicated by the error bars in Fig. 3B), there is no change in the total flux spontaneously generated at the tricrystal point at any temperature. Simple calculations indicate that, for example, an s-wave component to an $s + id$ superconducting order parameter would alter the flux quantization condition away from $\Phi_0/2$ by roughly the fractional portion that is s wave. We therefore conclude that the superconducting order parameter in YBCO is predominately d wave, with an imaginary component, if any, that is small from 0.5 K to T_c.

References and Notes

1. D. J. Scalapino, *Phys. Rep.* **250**, 329 (1995). An updated account of the phase-sensitive symmetry experiments appears in a review by C. C. Tsuei and J. R. Kirtley [*Physica C* **282–287**, 4 (1997)].
2. N. Bulut and D. J. Scalapino, *Phys. Rev. B* **54**, 14971 (1996).
3. S. M. Anlage *et al.*, *ibid.* **50**, 523 (1994).
4. J. Ma *et al.*, *Science* **267**, 862 (1995).
5. C. Kendziora, R. J. Kelley, M. Onellion, *Phys. Rev. Lett.* **77**, 727 (1996).
6. E. A. Pashitskii, V. I. Pentegov, A. V. Semenov, *Physica C* **282–287**, 1843 (1997).
7. N. E. Bickers, D. J. Scalapino, S. R. White, *Phys. Rev. Lett.* **62**, 961 (1989).
8. P. Monthoux, A. V. Balatsky, D. Pines, *Phys. Rev. B* **46**, 14803 (1992).
9. Conventional superconductors are invariant under time reversal. Certain possible unconventional pairing symmetries, such as $d_{x^2-y^2} + id_{xy}$, break this invariance.
10. S. Spielman *et al.*, *Phys. Rev. Lett.* **68**, 3472 (1992).
11. J. R. Kirtley *et al.*, *Nature* **373**, 225 (1995).
12. A. Mathai, Y. Gim, R. C. Black, A. Amar, F. C. Wellstood, *Phys. Rev. Lett.* **74**, 4523 (1995).
13. K. Suboki and M. Sigrist, *J. Phys. Soc. Jpn.* **65**, 3611 (1996).
14. M. Sigrist, D. B. Bailey, R. B. Laughlin, *Phys. Rev. Lett.* **74**, 3249 (1995).
15. M. Covington *et al.*, *ibid.* **79**, 277 (1997).
16. G. Koren, E. Polturak, N. Levy, G. Deutscher, N. D. Zakharov, *Appl. Phys. Lett.* **73**, 3673 (1998).
17. K. Krishana, N. P. Ong, Q. Li, G. D. Gu, N. Koshizuka, *Science* **277**, 83 (1997).
18. D. A. Wollman, D. J. van Harlingen, W. C. Lee, D. M. Ginsberg, A. J. Leggett, *Phys. Rev. Lett.* **71**, 2134 (1993).
19. D. A. Brawner and H. R. Ott, *Phys. Rev. B* **50**, 6530 (1994).
20. C. C. Tsuei *et al.*, *Phys. Rev. Lett.* **73**, 593 (1994).
21. J. H. Miller *et al.*, *ibid.* **74**, 2347 (1995).
22. J. R. Kirtley *et al.*, *Appl. Phys. Lett.* **74**, 4011 (1999).
23. These experiments use a Nb-AlO$_x$-Nb low-T_c SQUID with an integrated, well-shielded pickup loop. The SQUID is fabricated on a silicon substrate, which is connected through a highly thermally conducting copper cantilever and copper braid to the He$_4$ bath. The sample is scanned in relation to the SQUID with a lever mechanism. The sample and SQUID are in a vacuum space so that there is limited thermal conduction between them. The sample is heated with a thin-film resistor, and its temperature is measured with a silicon diode.
24. J. R. Kirtley *et al.*, *Phys. Rev. Lett.* **76**, 1336 (1996).
25. B. J. Roth, N. G. Sepulveda, J. P. Wikswo, *J. Appl. Phys.* **65**, 361 (1988).

26. We thank G. Trafas for sample fabrication and M. B. Ketchen and M. Bhushan for the design and fabrication, respectively, of the SQUIDs used in this experiment. We also thank A. J. Turberfield for suggesting the concept behind our variable temperature scanning SQUID microscope.

4 May 1999; accepted 13 July 1999

Inhibition of Crystallite Growth in the Sol-Gel Synthesis of Nanocrystalline Metal Oxides

Nae-Lih Wu,[1]* Sze-Yen Wang,[1] I. A. Rusakova[2]

Crystal growth upon firing of hydrous transition metal oxide gels can be effectively inhibited by replacing the surface hydroxyl group before firing with another functional group that does not condense and that can produce small, secondary-phase particles that restrict advancing of grain boundaries at elevated temperatures. Accordingly, fully crystallized SnO_2, TiO_2, and ZrO_2 materials with mean crystallite sizes of $\sim$20, 50, and 15 angstroms, respectively, were synthesized by replacing the hydroxyl group with methyl siloxyl before firing at 500°C. An ultrasensitive SnO_2-based chemical sensor resulting from the microstructural miniaturization was demonstrated.

Sol-gel synthesis is widely used for making transition metal oxide solids with fine-scaled microstructures. Pore and particle sizes no greater than a couple of nanometers can easily be achieved in the freshly derived gels. However, maintaining such microstructural dimensions when the fresh gels are subsequently crystallized at elevated temperatures is difficult. Freshly derived metal oxide gels have a hydrous solid skeleton that contains many hydroxyl groups and is either amorphous or paracrystalline. A postfiring step is therefore indispensable for dehydroxylation and for achieving a sufficient degree of crystallinity in order to give the desired combination of mechanical, catalytic, or optoelectronic properties for their applications. Upon firing of the gels, condensation among surface hydroxyl groups, nucleation of new oxide crystals, and growth of existing crystals occur concurrently over a fairly wide temperature range (*1*, *2*). Accordingly, some crystals grow extensively before the gel is fully dehydroxylated and crystallized, which reduces surface area, enlarges pores, and increases the difficulty of removing intracrystal defects.

In the preparation of SnO_2 oxidation catalyst, for example, firing of the hydrous gel at 400°C for 1 hour removes <80% of the hydroxyl content but has already led to a fivefold increase in crystal size, from $\sim$20 to 100 Å, and >50% loss in surface area and hence in catalytic activity (*2*). Firing hydrous ZrO_2 coating at 500°C is essential to giving sufficient thermomechanical strength for the high-temperature membrane reactor application, but pore sizes will more than triple, from 15 to 50 Å (see below). Destruction of the regular mesopore structures in the surfactant-templated metal oxide gels upon thermal treatment (*3*) is also likely caused by extensive crystal growth. Delayed crystal growth is thus the key to microstructural miniaturization of fully crystallized metal oxide materials prepared from the sol-gel and from other, similar wet processes.

Condensation of hydroxyl groups pulls together the constituent particles of the gel into a compact mass, and so the metal oxide crystals readily grow to a size much larger than that of the original particles. Accordingly, isolation of the hydrous particles upon firing may limit crystallization to taking place on a very local scale, and hence the original nanoscaled microstructure will be preserved. Second, crystal growth requires advancing of grain boundaries. Grain boundaries can be "pinned," and hence their motion restricted, by introducing tiny secondary-phase particles along grain boundaries. The challenge in the present case is to homogeneously introduce such "pinning" particles between crystals that are already nanoscaled. The surface hydroxyl groups appear to be perfect anchoring sites for the precursor species that would produce the particles. Therefore, an ideal approach that can simultaneously achieve both functions described above would be to replace the surface hydroxyl group with another functional group that does not condense as OH does and that could eventually form the "pins" at grain boundaries.

We tested this idea with particles of SnO_2, TiO_2, and ZrO_2, which are semiconducting ox-

[1]Department of Chemical Engineering, National Taiwan University, Taipei, Taiwan 106, Republic of China. [2]Texas Center for Superconductivity at the University of Houston, Houston, TX 77204–5932, USA.

*To whom correspondence should be addressed. E-mail: nlw001@coms.ntu.edu.tw